



The Journal of Pharmacology and Experimental Therapeutics





journal homepage: www.jpvet.aspetjournals.org



ARTICLE

Morphine-induced hyperalgesia impacts small extracellular vesicle microRNA composition and function



Deepa Reddy ¹ , Zhucheng Lin ¹, Sujay Ramanathan ¹, Xuan Luo ¹, Richa Pande ² ,
Yuzhen Tian ¹, Christine M. Side ¹, Jacqueline M. Barker ¹ , Ahmet Sacan ³ ,
Julie A. Blendy ⁴, Seena K. Ajit ^{1,*}

¹ Department of Pharmacology & Physiology, Drexel University College of Medicine, Philadelphia, Pennsylvania

² Microbiology and Immunology Graduate Program, Drexel University College of Medicine, Philadelphia, Pennsylvania

³ School of Biomedical Engineering, Science & Health Systems, Drexel University, Philadelphia, Pennsylvania

⁴ Department of Systems Pharmacology and Translational Therapeutics, Perelman School of Medicine, University of Pennsylvania, Philadelphia, Pennsylvania

ARTICLE INFO

Article history:

Received 22 October 2024

Accepted 30 January 2025

Available online 6 February 2025

Key words:

Small extracellular vesicles

MicroRNA

Morphine

Opioid-induced hyperalgesia

CREB


ABSTRACT

Morphine and other synthetic opioids are widely prescribed to treat pain. Prolonged morphine exposure can paradoxically enhance pain sensitivity in humans and nociceptive behavior in rodents. To better understand the molecular mechanisms underlying opioid-induced hyperalgesia, we investigated changes in microRNA (miRNA) composition of small extracellular vesicles (sEVs) from the serum of mice after a morphine treatment paradigm that induces hyperalgesia. We observed significant differential expression of 18 miRNAs in sEVs from morphine-treated mice of both sexes compared with controls. Several of these miRNAs were bioinformatically predicted to regulate cyclic AMP response element binding protein (CREB), a well characterized transcription factor implicated in pain and drug addiction. We confirmed the binding and repression of *Creb* mRNA by miR-155 and miR-10a. We tested if serum-derived sEVs from morphine-treated mice could elicit nociceptive behavior in naïve recipient mice. Intrathecal injection of 1 μ g sEVs did not significantly impact basal mechanical and thermal thresholds in naïve recipient mice. However, prophylactic 1 μ g sEV administration in recipient mice resulted in faster resolution of complete Freund's adjuvant-induced mechanical and thermal inflammatory hypersensitivity. Other behaviors assayed following administration of these sEVs were not impacted, including sEV-conditioned place preference and locomotor sensitization. These results indicate that morphine regulation of serum sEV composition can contribute to analgesia and suggest a potential for sEVs to be a nonopioid therapeutic intervention strategy to treat pain.

Significance Statement: A mouse model of opioid-induced hyperalgesia was used to show that chronic morphine treatment causes differential microRNA packaging into small extracellular vesicles (sEVs) present in the serum of mice. Two of these sEV microRNAs can downregulate CREB expression, and administration of these sEVs attenuates pain hypersensitivity in recipient mice. These studies position sEVs as a potential pain therapeutic and highlight changes underlying opioid-induced hyperalgesia, shedding light on a phenomenon with unclear pathophysiology.

© 2025 The Author(s). Published by Elsevier Inc. on behalf of American Society for Pharmacology and Experimental Therapeutics. This is an open access article under the CC BY-NC-ND license (<http://creativecommons.org/licenses/by-nc-nd/4.0/>).

* Address correspondence to: Dr Seena K. Ajit, Department of Pharmacology & Physiology, Drexel University College of Medicine, 245 North 15th Street, Mail Stop 488, Room 8223, Philadelphia, PA 19102. E-mail: ska52@drexel.edu

 This article has supplemental material available at jpvet.aspetjournals.org.

D.R., Z. L., and S.R. contributed equally to this work.

1. Introduction

Chronic pain affects more than 100 million people in the United States, with the annual cost to society estimated at \$635 billion (Gereau *et al*, 2014). Morphine and other synthetic opioids are widely prescribed to treat pain, but their continued use can induce a progressive decrease in analgesia (tolerance) and the development of hypersensitivity to painful stimuli, or opioid-induced

hyperalgesia (OIH) (Chu et al, 2008; Roeckel et al, 2016). Thus, the treatment meant to relieve pain will paradoxically exacerbate pain. This vicious cycle can lead some patients to develop drug addiction or abuse with negative consequences, severely complicating the management of chronic pain (Angst and Clark, 2006; Lee et al, 2011). Although multidisciplinary approaches including opioid rotation, opioid tapering, and incorporating nonopioid analgesics and nonpharmacological interventions are pursued, OIH remains an unmet clinical need (Colvin et al, 2019), and the mechanisms underlying OIH are not well understood.

Secreted membrane-enclosed vesicles, collectively called extracellular vesicles (EVs), include exosomes, microvesicles, apoptotic bodies, and other EV subsets (Couch et al, 2021). Small EVs (sEVs), predominantly exosomes, have been implicated in their role in mediating intercellular communication. sEVs are 30–150 nm vesicles that transport biomolecules, including microRNAs (miRNAs), mRNAs, proteins, and lipids in bodily fluids (van Niel et al, 2018; Couch et al, 2021). sEVs do not incorporate at random or everything present in the parental cell cytoplasm, suggesting that their synthesis is a well regulated process that can be dynamically altered by signaling cues (Thery et al, 2009). sEVs can cross the blood-brain barrier and have gained significant attention in recent years for their biomarker potential (D'Agnelli et al, 2020; Hornung et al, 2020). They can mediate communication in the nervous system, which may supplement the known mechanisms of anterograde and retrograde signaling across synapses (Zappulli et al, 2016). While sEVs can have a detrimental role in neurodegenerative disorders (Hartmann et al, 2017), they can also have protective functions. We and others have shown anti-inflammatory (Kim et al, 2005) and antinociceptive effects (McDonald et al, 2014; Jean-Toussaint et al, 2021) of sEVs derived from antigen-presenting cells.

Opioids have been reported to alter cargo composition in sEVs and studied in the context of substance use disorder and human immunodeficiency virus infection (Odegaard et al, 2020; Caobi et al, 2023). A few studies have investigated the impact of morphine treatment on sEV cargo composition. Exposure of astrocytes to morphine resulted in a significant increase in the number of sEVs released compared with control cells (Hu et al, 2018). sEVs from morphine-treated astrocytes also showed alterations in miRNA composition, and 15 of the upregulated miRNAs were linked to the inhibition of morphine-mediated phagocytosis in recipient microglial cells (Hu et al, 2018). They also reported that morphine-mediated dysregulation of miRNA cargo in astrocyte-derived sEVs led to pericyte migration and loss of pericyte coverage, and this effect was mediated by miR-23a in a mu-receptor-dependent manner (Liao et al, 2022).

In rodents, the administration of opioids by subcutaneous morphine pellet implantation, subcutaneous injections, osmotic minipumps, or infusions through intrathecal catheters for 3–12 days results in antinociception typically on the first day, followed by a loss of this effect and progressive hyperalgesia to thermal or mechanical stimuli over the course of several days (Ossipov et al, 2004; Angst and Clark, 2006; Arout et al, 2015). Previous studies have shown that subcutaneous pellet implantation produced prolonged and robust OIH (Li et al, 2001; Liang et al, 2008; Chen et al, 2010) and dependence as measured by significant increases in somatic signs of withdrawal (Maldonado et al, 1996; Walters and Blendy, 2001). Here we investigated chronic morphine-induced changes in miRNA composition in sEVs from the serum of mice after a morphine treatment paradigm that induces hyperalgesia. Our previous studies using sEVs from either RAW 264.7 macrophage cell line or the serum of donor mice (both naïve and neuropathic pain model) showed that administering these sEVs in recipient mice contributed to faster resolution of inflammatory

pain hypersensitivity (Jean-Toussaint et al, 2021; Lin et al, 2025). We hypothesized that sEVs from the OIH model would elicit a similar response in recipient mice. Here we tested whether intrathecally administering sEVs from the OIH model contributes to analgesia in morphine-naïve recipient mice and prophylactically in a mouse model of inflammatory pain. Given that morphine also has central nervous system effects, we wanted to determine if the sEVs from morphine-treated mice would affect locomotor activity and behavioral sensitization and tested this by injecting sEV into the ventral tegmental area (VTA) of recipient mice.

2. Materials and methods

2.1. Mice

All the studies were performed following the National Institute of Health guidelines, and the protocols were approved by the Institutional Animal Care and Use Committee of Drexel University College of Medicine and the University of Pennsylvania. Eight- to 10-week-old male and female C57BL/6J mice were purchased from the Jackson Laboratory. Mice were housed in a 12-hour light/dark cycle and provided with food and water ad libitum.

2.2. Mouse models of pain and behavioral testing

For the OIH model by morphine pellet implantation, a morphine (75 mg morphine base) pellet or placebo (cellulose) pellet (National Institute on Drug Abuse Supply Program) was implanted subcutaneously on the dorsal surface of mice under general isoflurane anesthesia. For the OIH model of morphine injections, morphine (#15464, Cayman Chemical) was resuspended in DMSO and diluted with sterile PBS to a concentration of 10 mg/mL. Mice were subcutaneously injected twice daily with 20 mg/kg on days 1–3 and 40 mg/kg on day 4 as previously reported (Liang et al, 2019). For complete Freund's adjuvant (CFA) model of inflammatory pain, mice were injected subcutaneously with 20 μ L of 50% emulsified CFA (Sigma-Aldrich) in PBS into the plantar hind paw.

Mice were habituated in behavioral testing rooms at least 4 days before baseline tests. The experimenters were blinded to the treatment conditions. Mechanical sensitivity was determined using the von Frey test. Static mechanical paw withdrawal thresholds were assessed by applying graded von Frey monofilaments to the plantar surface of the paw. The paw withdrawal threshold was determined and evaluated by the up-down method (Deuis et al, 2017). Baseline measurements were taken for 3 days before any injection was administered, and the values were averaged. The Hargreaves test was used to assess thermal sensitivity (Jean-Toussaint et al, 2021). The baseline latencies were taken for 3 days before any injection was administered and were adjusted to approximately 10 seconds with a maximum of 20 seconds as the cutoff to prevent potential injury. Animals were placed on a plexiglass platform, and a thermal beam was applied to the hind paw using an infrared light source under the plexiglass platform. The latency for the mice to withdraw their paws in pain was recorded as its threshold. Tail-flick assays were performed as reported (Bannon and Malmberg, 2007). Briefly, the mouse tail was marked at 3 different points. The animal was restrained on the tail-flick test analgesia meter (Columbus Instruments) such that each marking was placed in the center of an intense light beam focused on the tail, and the latency for the mice to flick its tail in pain was recorded as its threshold. The average of 3 different timings from each location on the tail was plotted. The latency at the first marking was done on all animals, followed by the second marking on all animals then the third to ensure the accuracy of results. The heat intensity

was adjusted to evoke a tail-flick baseline latency of ~10 seconds. A cutoff time was set at 20 seconds to avoid tissue damage.

2.3. Locomotor activity and behavior sensitization

Locomotor activity was analyzed in a home cage activity monitoring system (Med Associates Inc). The testing cage, identical in dimension to the home cage, was placed in a photobeam frame (30 cm × 24 cm × 8 cm) with 2 levels of sensors arranged in an 8-beam array strip. For locomotor sensitization, animals were tested every 2–3 days for 120 minutes following an injection of saline or morphine (10 mg/kg, s.c.). On treatment days 1–3, all animals were administered saline. On days 4–9, animals received either morphine or saline, according to their treatment group. One microgram of sEVs was injected 24 hours before day 1. Beam break data were read into Med Associates' personal computer-designed software and monitored at 10-minute intervals.

2.4. Conditioned place preference

Morphine-naïve adult male C57BL/6J mice (n = 8/group) underwent conditioned place preference (CPP) training and testing to determine if sEVs derived from morphine-treated mice elicit a context-reward association compared with sEVs derived from naïve mice. Training and testing took place in standard 3-chamber CPP boxes with retractable doors (Med Associates Inc). Each box consisted of 1 black chamber with grid floors, 1 white chamber with wire mesh floors, and a smaller central gray chamber with solid floor. The time spent and locomotor behavior in each chamber were automatically detected using photocell beam breaks, calculated using custom code for Med-PC V software (Med Associates Inc). During a preconditioning session, mice were placed in the neutral chamber and allowed to freely explore all 3 chambers for 20 minutes. Using a biased design, the less-preferred chamber was assigned to be paired with sEV treatment. For the first conditioning session, all mice received an intrathecal injection of the vehicle 1 hour prior to confinement in the vehicle-paired chamber for an hour. On the following day, mice were assigned based on initial preference to receive an intrathecal injection of vehicle, sEVs from naïve, or morphine-treated mice 1 hour prior to confinement to the sEV-paired chamber. This timing was selected to minimize the effects of the intrathecal injection itself on the development of a CPP and to reduce any carryover effect of sEV injection on subsequent conditioning sessions. Only a single sEV injection was used in order to reflect the behavioral paradigm. One day after the sEV-conditioning sessions, mice were returned to the boxes by an experimenter blinded to the treatment condition and were allowed to freely explore for 20 minutes in a test session identical to the preconditioning session. To control for initial side preference in this biased design, the CPP score was calculated by subtracting the time spent (seconds) during preconditioning from the time spent during CPP assessment.

2.5. Intrathecal sEV administration

Eight to 10-week-old C57BL/6J mice were used for intrathecal injections. All injections were performed with a Hamilton syringe and 30-gauge needles. After identification of the injection site, the needle was inserted into the tissue to the intervertebral space between L4 and L5, and a successful puncture resulted in a tail flick. Then, 10–15 μ L of 1 μ g sEVs or sterile PBS was slowly injected.

2.6. VTA injection of green PKH67 labeled sEVs

Fluorescent labeling of sEVs was performed with general lipophilic fluorescent membrane dye, PKH67, according to the manufacturer's instructions (Sigma-Aldrich). Mice were anesthetized with isoflurane and placed in a stereotax. Mice received subcutaneous meloxicam (2 mg/kg) on the day of surgery. PKH67-labeled sEVs were injected in the mouse VTA (anteroposterior –3.4, lateral –0.3, and dorsoventral –4.4) (Paxinos and Franklin, 2007).

2.7. Isolation of sEVs from mouse serum

The serum for sEV isolation was obtained from mice 6 days post morphine or placebo pellet implantation and 5 days post first subcutaneous morphine or saline injections. A combination of differential ultracentrifugation, ultrafiltration, and size-exclusion chromatography was used to isolate sEVs from mouse serum. All centrifugations were performed at 4 °C. Briefly, the OIH model or control mice were anesthetized using isoflurane. Whole blood was collected via the eye in 1.7 mL microcentrifuge tubes without anticoagulant and incubated undisturbed at room temperature for 45 minutes to allow clot formation. The supernatant serum was collected after centrifugation at 2000 × g for 10 minutes and stored at –80 °C until use. The serum sample was diluted with an equal volume of Dulbecco's PBS (DPBS) without calcium and magnesium and then centrifuged for 30 minutes at 2000 × g to pellet cell debris. The supernatants were then centrifuged at 12,000 × g for 45 minutes, and the suspension was filtered through a 0.22- μ m syringe filter. Samples were then diluted to 4 mL with DPBS and transferred to 100 K Amicon Ultra Centrifugal Filters (Sigma-Aldrich), followed by centrifugation at 5000 × g for 30 minutes. The concentrate was diluted to 500 μ L with DPBS and purified using size-exclusion chromatography using qEV original 35 nm Legacy columns (iZON) following the manufacturer's instructions. Four EV-rich fractions (7–10, 0.5 mL each) were pooled, and after ultracentrifugation at 110,000 × g for 70 minutes (Optima TLX ultracentrifuge with TLA 100.4 rotor, Beckman Coulter Inc), the pellets were resuspended in DPBS and stored at –80 °C until further use.

2.8. Nanoparticle tracking analysis

Brownian motion of sEV particles from mouse serum was visualized, and size distribution and concentration of sEVs were measured using NanoSight NS300 (Malvern Instruments). Briefly, sEV samples were diluted in DPBS and placed into the sample chamber using a syringe pump. The combination of shutter speed and gain was set to obtain 30-second videos, which were analyzed using the NanoSight NTA 3.1.54 software (Malvern Panalytical Inc).

2.9. Detection of sEV surface epitopes using flow cytometry

The mouse MACSPlex exosome kit (#130-122-211, Miltenyi Biotec) was used to detect sEV-specific markers using BD LSRFortessa (BD Biosciences) following the manufacturer's protocol using 10 μ g of sEVs as previously described (Lin et al, 2025). Positive percentage (%Pos) of the IgG control was subtracted from each marker's %Pos to remove background. To better represent both differences in percent positive and geometric mean fluorescent intensity (MFI), MFI for each marker was normalized to the highest observed MFI across the groups. Weighted expression was calculated as (%Pos < 60%) = % Pos, (Values \geq %Pos 60%) = ([MFI/Highest MFI across groups] × % Pos × 0.5) + [Percent Positive × 0.5]), where 0.5 represents equal weighting of % Pos and weighted MFI expression. Samples are represented in the form of a heat map.

2.10. miRNA profiling of sEVs and pathway analysis

Total RNA was isolated from sEVs using Ambion *mirVana* miRNA isolation kit (Life Technologies) following the manufacturer's protocol. miRNA profiling was performed as described previously (Ramanathan et al, 2019a) using rodent TaqMan low-density array microfluidic cards version A and B (Applied Biosystems) in 100 ng of total RNA. Undetermined cycle threshold (CT) values were first set to 40. Low-expressed or undetected miRNAs with an average CT value of greater than 35 in all experimental groups were removed from the analysis. A miRNA was considered present in 1 experimental group only when the CT value of each replicate was lower than 35. Fold change was calculated from raw CT values using the $2^{-\Delta\Delta CT}$ method (Schmittgen and Livak, 2008). The mean CT values of the top 10 miRNAs with the lowest standard deviations across all samples were used as the baseline CT for calculating the normalized ΔCT values. Statistical significance of differences in ΔCT values was determined using a two-tailed *t* test for comparison of serum-derived sEVs from morphine-treated and control mice. A *P* value threshold of .05 and an absolute fold change of 2 were used to select significantly differentially expressed miRNAs between experimental groups.

Genes targeted by differentially expressed miRNAs were identified using the union of the computationally predicted targets in TargetScan (with a Pct score of at least 0.90) (McGeary et al, 2019) and the experimentally validated targets in miRTarBase (Huang et al, 2022). Gene set enrichment analysis of the resulting targeted genes was done using ShinyGO 0.80 (Ge et al, 2020) to identify Gene Ontology (GO) biological processes and Kyoto Encyclopedia of Genes and Genomes pathways. To reduce the redundancy among the reported GO biological processes, we applied a filtering where GO terms sharing more than 90% of their genes were removed, keeping only the GO terms with the most significant false discovery rate value.

2.11. Cell culture

Human embryonic kidney 293 and RAW 264.7 cells (American Type Culture Collection) were grown in complete media (Dulbecco's modified Eagle's medium, Corning) supplemented with 10% heat-inactivated fetal bovine serum (Corning) and 1% penicillin/streptomycin (Gibco) at 37 °C in 5% CO₂.

2.12. Luciferase reporter assay

The 3'-untranslated region (UTR) of mouse *Creb1* (NM_133828.2) is 6912 bp long, exceeding the capacity of the luciferase vector plasmid. Hence, the *Creb* 3'-UTR was cloned as 3 separate and overlapping fragments downstream of the luciferase gene to generate 3 constructs. Human embryonic kidney 293 cells were transfected with precursor miRNA for miR-155, miR-10a, or scrambled control, and luciferase reporter plasmid containing the 3'-UTR plasmid using Lipofectamine 2000 (Life Technologies) for 48 hours. The Luc-Pair miR Luciferase assay kit (GeneCopoeia) was used to measure firefly and Renilla luciferase activity according to the manufacturer's protocol. Firefly luciferase measurements normalized to Renilla were used as a transfection control. The data are the average of 3 independent experiments.

2.13. Overexpression of miRNAs in RAW 264.7 cells

Lipofectamine RNAiMax transfection reagent (Life Technologies) was used for miRNA transfections and performed according to the manufacturer's protocol as described before

(Ramanathan et al, 2019a). After 24 hours, cell pellets were washed with 1 × PBS and resuspended in either RNA lysis buffer (*mirVana* kit) containing 0.5 U/μL RNasin Plus (Promega) for RNA isolation or 1X radioimmunoprecipitation assay buffer containing protease inhibitor cocktail (Thermo Scientific) for protein analysis.

2.14. Cellular RNA isolation and quantitative polymerase chain reaction

Total RNA was isolated using the *mirVana* RNA isolation kit. RNA concentrations were determined using a NanoDrop ND1000 spectrophotometer (NanoDrop Technology Inc). The Maxima cDNA synthesis kit (Thermo Fisher Scientific) was used to generate cDNA and 1 μL cDNA was used for mRNA quantitative polymerase chain reaction (qPCR) analysis. *Gapdh* (#4352339E, Applied Biosystems) was used as the normalizer. The primer probe used for *Creb1* was Mm00501607_m1 (Applied Biosystems).

2.15. Western blotting

Cell or sEV samples were resuspended in radioimmunoprecipitation assay buffer (1:1) (Sigma-Aldrich) with protease inhibitors (1:100). Protein concentrations were measured using the Micro BCA Protein Assay kit (Thermo Scientific) for sEVs or the detergent compatible protein assay (Bio-Rad) for cell lysates. Equal amounts of protein samples in Laemmli SDS sample buffer (Thermo Scientific) were loaded on 10% Tris-Glycine gel (Thermo Scientific), and the gel was run at 125 V for 90 minutes. Proteins were transferred to a 0.4-μm polyvinylidene fluoride membrane at 25 V for 90 minutes, followed by blocking the membrane with 5% milk in Tris-buffered saline with 0.1% Tween-20 (TBST) blocking buffer for 1 hour at room temperature. The membranes were incubated with primary antibodies in TBST and 10% (v/v) blocking buffer on a shaker overnight at 4 °C. The blots were washed with TBST thrice, 5 minutes each, and then the blots were incubated with secondary antibodies in TBST at room temperature for 1 hour on the shaker. The membranes were washed with TBST thrice, and protein was detected using LI-COR Image Studio Software (LI-COR Biosciences). Primary antibodies used were rabbit anti-albumin (1:2000, #16475-1-ap, Proteintech), rabbit anti-CREB (48H2) antibody (1:1000, #9197S, Cell Signaling), and mouse anti-β-actin (8H10D10) antibody (1:1000, #3700T, Cell Signaling). Secondary antibodies used were goat anti-rabbit horseradish peroxidase conjugate (1:10,000, #170-6515, Bio-Rad) and goat anti-mouse horseradish peroxidase conjugate (1:10,000, #170-6516, Bio-Rad). The blots were developed using the SuperSignal West Femto substrate (Thermo Fischer).

2.16. Statistical analysis

Data are presented as mean ± SEM from 3 or more independent experiments. Student *t* test was used to determine the statistical significance for in vitro studies. Treatment effects were analyzed with a one-way ANOVA and the multiple comparisons between means were tested using the post hoc Bonferroni method. All behavior data were analyzed using two-way ANOVA, and pairwise comparisons between means were tested using the post hoc Šidák test. The differences between groups were considered significant when the *P* value was less than .05. GraphPad Prism software (versions 10 and 11; GraphPad) was used for all statistical analysis.

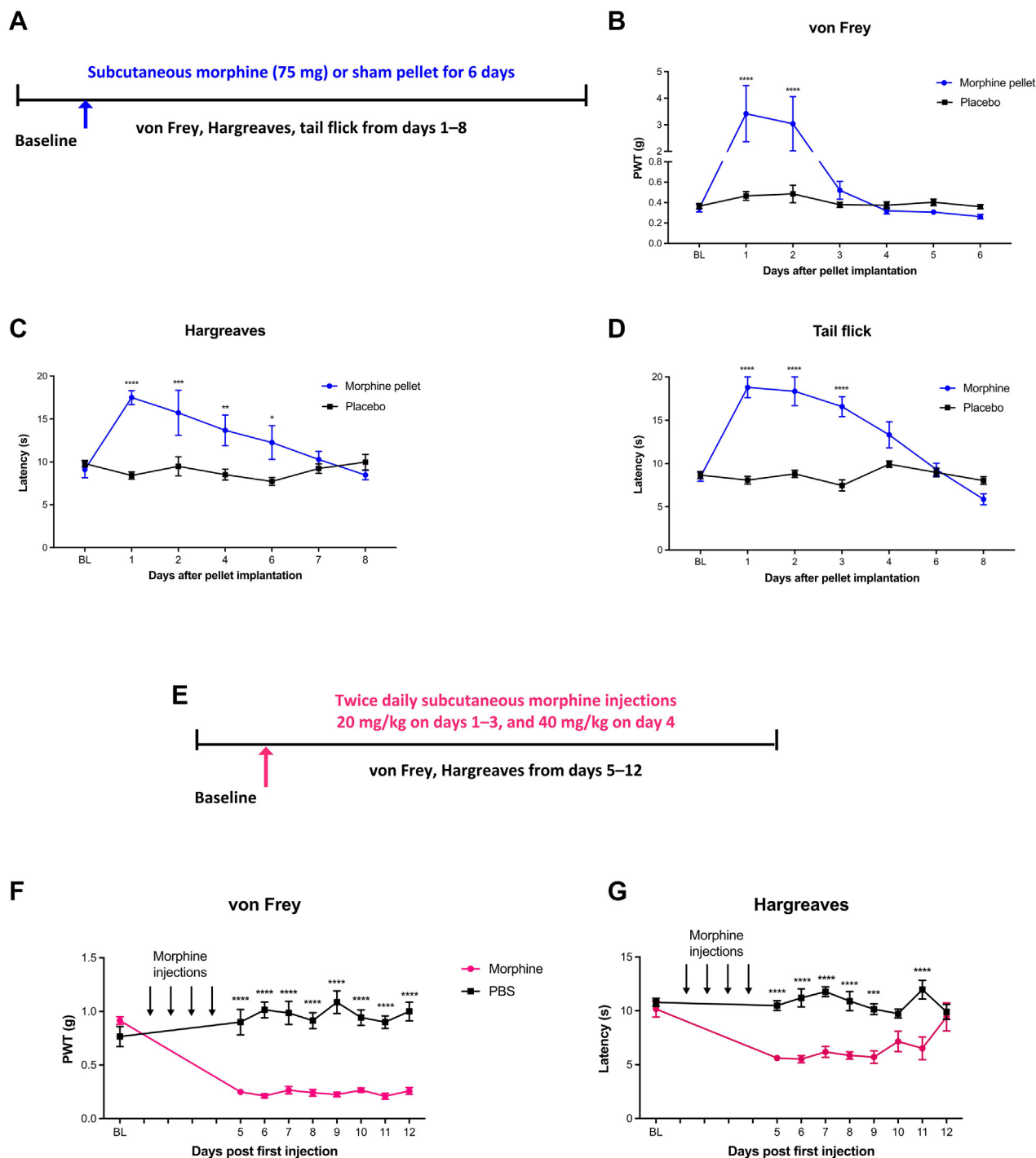


Fig. 1. Morphine-induced OIH in mice. (A) Schematic representation of chronic morphine-induced hyperalgesia model using subcutaneous implantation of 75 mg morphine or a placebo pellet. (B) Mechanical allodynia was determined using the von Frey test, and thermal hyperalgesia was assessed using the (C) Hargreaves test, and (D) the tail-flick assay in mice implanted with a morphine pellet. (E) Schematic of escalating doses of morphine (20 mg/kg twice daily for 3 days and 40 mg/kg on the 4th day, s.c.) model for OIH. (F) Mechanical allodynia and (G) thermal hyperalgesia in mice receiving escalating doses of morphine. Ten-week-old male C57BL/6J mice were used ($n = 7$). Statistical analysis was determined by two-way repeated measures ANOVA followed by Sidak's multiple comparisons test; * $P < .05$, ** $P < .01$, *** $P < .001$, **** $P < .0001$. BL, baseline; PWT, paw withdrawal threshold.

3. Results

3.1. Effect of chronic morphine treatment on mechanical and thermal threshold

To study the changes in sEV composition under morphine-induced hyperalgesia compared with control sEVs, we isolated

sEVs from mouse serum. Subcutaneous morphine pellet implantation and repeated morphine injections are both used to generate OIH models, so we investigated the development of chronic morphine-induced hyperalgesia using both methods. Subcutaneous morphine pellet implantation causes prolonged and robust OIH (Li et al, 2001; Liang et al, 2008; Chen et al, 2010). The study schematic following 75 mg morphine or a placebo (cellulose) pellet

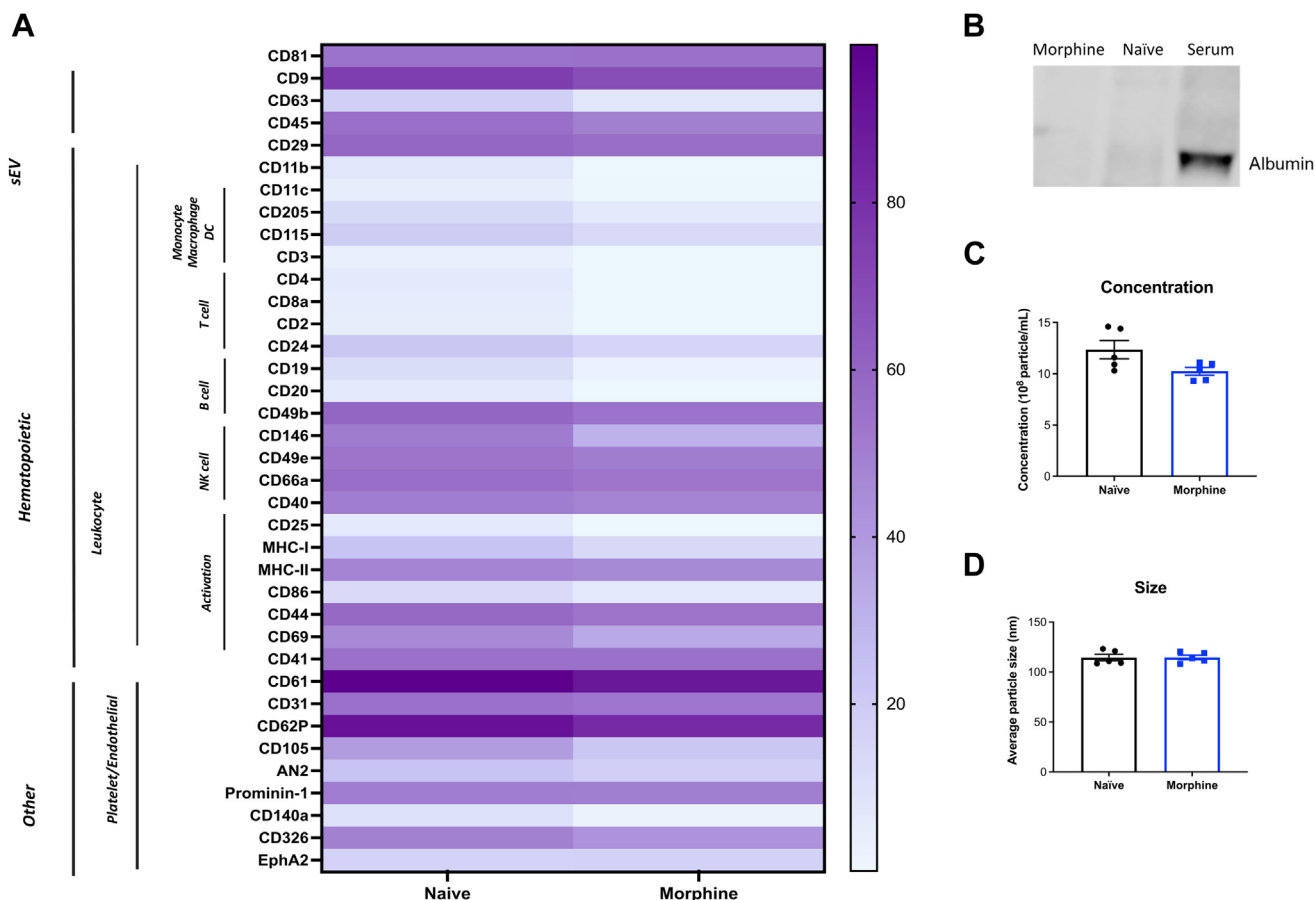


Fig. 2. Characterization of sEVs purified from mouse serum. (A) Characterization of markers on serum-derived sEVs from naïve and OIH mice using a MACSPlex flow cytometry bead-based capture and fluorescent detection assay. sEVs ($n = 1$) used were from a pool of serum of 5 mice of each treatment. Comparisons are normalized and weighted to represent alterations in both percent positive and fluorescent intensity. (B) Western blot analysis of sEV lysate show that albumin is absent in sEV samples, indicating purity. (C) Nanoparticle tracking analysis of naïve- and morphine-derived sEVs indicated mean concentrations of $12.36 \pm 2.01 \times 10^8$ and $10.25 \pm 0.85 \times 10^8$ particles/mL, respectively; and (D) mean diameters of 114.48 ± 7.05 and 114.58 ± 5.15 nm, respectively, indicating purity. DC, dendritic cells; NK, natural killer cells.

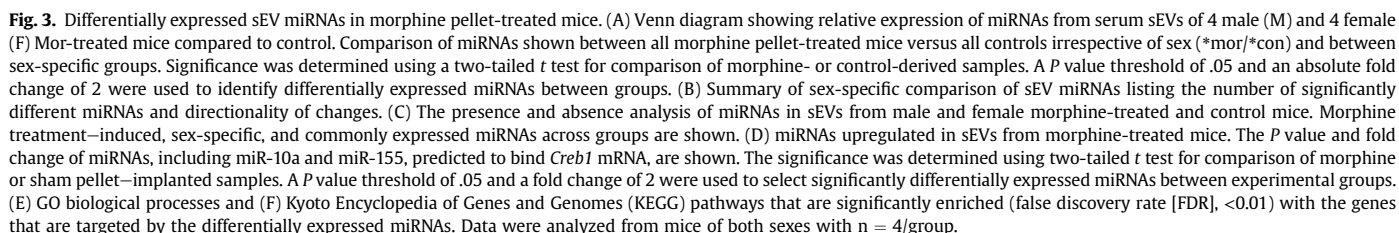
implantation is shown in Fig. 1A. As expected, morphine-induced antinociception with an increase in mechanical threshold in the von Frey test, but this effect was lost by day 4 (Fig. 1B). Assessment of thermal sensitivity as determined using the Hargraves test (Fig. 1C) and tail-flick assay (Fig. 1D) showed highest paw withdrawal latency times on day 1, which diminished gradually. This was followed by a decrease in paw withdrawal latency comparable to the control group. In mice that received subcutaneous morphine injections for 4 days (Liang et al, 2019) (Fig. 1E), mechanical allodynia (Fig. 1F) and thermal hyperalgesia (Fig. 1G) developed on day 5, and thermal hyperalgesia lasted for 12 days. Overall, our studies confirmed previous observations (Chen et al, 2010) that continuous morphine treatment induced mechanical allodynia and thermal hyperalgesia.

3.2. Characterization of serum-derived sEVs

sEVs were characterized for the presence or enrichment of endosome-derived membrane proteins such as tetraspanins and assessed using bead-based flow cytometry. In addition to confirming the expression of tetraspanin proteins, we also observed that though the sEVs from the serum of morphine-treated (Mor-sEVs) and naïve mice (naïve-sEVs) had a similar expression, the expression of CD146, CD69, and CD105 was lower in Mor-sEVs (Fig. 2A). We also confirmed the purity of sEVs using western blot analysis for the negative control protein albumin, which is detected

in the serum but absent in sEVs (Fig. 2B). We performed nanoparticle tracking analysis of serum-derived sEVs and observed the mean concentrations of naïve-sEVs and Mor-sEVs to be $12.36 \pm 2.01 \times 10^8$ and $10.25 \pm 0.85 \times 10^8$ particles/mL, respectively (Fig. 2C). The mean diameters were less than 150 nm (Fig. 2D), indicating these vesicle preparations fall within the size range of sEVs. There was no statistical difference between sEVs from controls or morphine-treated mice.

miRNA composition differs in sEVs purified from serum of morphine-treated mice versus control mice. We investigated chronic morphine-induced changes in miRNA composition of sEVs in the serum. Both male ($n = 5$ /group) and female ($n = 4$ /group) mice were included to identify sex-specific differences. Profiling of 758 miRNAs using qPCR (Supplemental Table 1) showed significant differential expression of 18 miRNAs in sEVs from morphine-treated mice compared to control. The Venn diagram summarizes the number of sex-specific miRNAs that are significantly altered (Fig. 3A), and the number of miRNAs up or downregulated in Mor-sEVs is shown (Fig. 3B). Presence-absence analysis showed that all the miRNAs expressed in the female OIH model were found in the female control (Fig. 3C, Supplemental Table 2). However, the male OIH model had 15 exclusively present and 16 exclusively absent miRNAs compared with the same-sex control. These suggest that the male OIH model has a specific miRNA signature. There are 37 commonly expressed miRNAs across all the groups. Figure 3D shows miRNAs upregulated in Mor-sEVs, and Supplemental Table 3



lists all significantly altered miRNAs and the corresponding fold changes and *P* values.

Biological processes and pathways regulated by the differentially expressed miRNAs irrespective of sex were identified by compiling the target genes of these miRNAs, followed by gene set enrichment analysis. Major categories of enriched biological processes included regulation of nitrogen metabolism, developmental processes, response to stimulus, and signaling (Fig. 3E, Supplemental Table 4). Pathway enrichment analysis indicated that the genes regulated by the miRNAs that are differentially expressed in morphine-treated mice are also involved in various cancers and signaling pathways, including mTOR, MAPK, Wnt, and PI3K-Akt (Fig. 3F). In Supplemental Table 5 and Supplemental Fig. 1, GO shows the subsets of the significantly enriched biological processes that CREB1 is involved in.

3.3. Confirmation of miRNA binding to the 3'-UTR of *Creb1* and transcriptional regulation of target genes

Small noncoding miRNAs regulate gene expression by binding predominantly to the 3'-UTR of mRNAs via a 6–8-bp seed sequence complementarity. We performed bioinformatic analysis of miRNAs upregulated in sEVs from morphine-treated mice and observed that several of the miRNAs are predicted to target *Creb1* mRNA. Because there were multiple miRNAs predicted to target *Creb1* 3'-UTR, including some miRNA target sites represented more than once, we selected 2 miRNAs, miR-155 and miR-10a, that were significantly upregulated in the morphine group as a whole (male and female mice combined) versus the control group (Fig. 3D). miR-132 is another miRNA that we identified, and previous studies have validated that miR-132 binds to and negatively regulates *Creb1* (Klein et al, 2007).

Upon binding, miRNAs can induce either mRNA degradation or translational repression and thus negatively regulate the expression of target genes (Bartel, 2009; Wilczynska and Bushell, 2015). To confirm miRNA binding to the 3'-UTR of *Creb1*, we performed a luciferase reporter assay. Because the *Creb1* 3'-UTR is ~7 kb, we cloned it as 3 separate fragments (*Creb1*-1, -2, and -3, schematic shown in Fig. 4A) to test them for miRNA binding in the reporter assay. Fig. 4B shows the reduction in luciferase activity 48 hours after transfection of miR-10a and miR-155. miR-10a has binding sites present in fragments “2” and “3,” but more efficient binding was observed in fragment “3” compared with fragment “2.”

To test the ability of miR-155 and miR-10a to modulate endogenous *Creb1* mRNAs in vitro, we transfected mouse RAW 264.7 macrophage cells with miRNA mimics or scrambled control miRNA. Because miRNAs can regulate gene expression by mRNA degradation or translational repression, we performed qPCR to measure endogenous levels of target mRNAs 24 hours after transfection. There was a reduction in *Creb1* mRNA levels upon miRNA transfection, suggesting that miR-155 and miR-10a binding can down-regulate *Creb1* (Fig. 4C). To further confirm that miR-155 and miR-10a can negatively regulate protein expression of CREB1, a western blot analysis of RAW 264.7 macrophage cell lysate 24 hours after miRNA transfection was performed. Figure 4D shows that overexpression of these miRNA mimics resulted in lower levels of CREB protein, and there was an additive effect upon transfection with both miRNAs, which was more evident in the qPCR findings (Fig. 4C).

3.4. Prophylactic intrathecal administration of sEVs isolated from chronic morphine-treated mice attenuates thermal hypersensitivity

To investigate the role of sEVs released during chronic morphine exposure in modulating pain, we tested if exogenously

administering 1 μ g of sEVs from morphine-treated or control mice intrathecally into naïve male recipient mice can modulate basal pain thresholds. A schematic of the paradigm is shown in Fig. 5A. We tested the effect of sEVs on basal threshold using sEVs from both morphine pellet–implanted (Fig. 5, B–E) and morphine-injected (Fig. 5, F–J) models along with their respective control mice. We observed that 1 μ g of mouse serum–derived sEVs obtained from morphine pellet–implanted male sEV OIH model donor mice, when administered intrathecally into drug-naïve male recipient mice, resulted in an increase in thermal (Fig. 5C), but not mechanical (Fig. 5B), paw withdrawal latency. This indicates elevated pain thresholds on day 3 in mice treated with Mor-sEVs from the pellet model OIH mice. However, Mor-sEVs from morphine injection model mice did not alter basal pain thresholds in recipient mice (Fig. 5, F and G). We also tested the efficacy of sEVs from morphine injection OIH model mice in a tail-flick model to assess the analgesic effect to thermal stimuli and did not observe any significant difference at 3 hours after sEV injection (Supplemental Fig. 2). We then investigated how prophylactic administration of these sEVs impacted nociceptive threshold to a future painful stimulus. Inflammatory pain was induced by an intraplantar injection of CFA 10 days after sEV administration. Irrespective of the method (morphine pellet or injection) used to induce OIH, mice injected with Mor-sEVs showed attenuation of CFA-induced thermal hypersensitivity (Fig. 5, E and I). There was also a significant attenuation of CFA-induced mechanical hypersensitivity in mice treated with Mor-sEVs from the OIH injection model as compared with control (Fig. 5H), but not in the mice that received OIH pellet model-derived sEVs (Fig. 5D).

3.5. Behavior response to morphine administration in sEV-treated mice

Behavioral sensitization serves as an important model of neural plasticity and has been suggested as a mechanism that may model aspects of human drug addiction (Robinson and Berridge, 1993). We have previously used locomotor activity to study the sensitizing effects of morphine (Walters et al, 2003, 2005b; Mague et al, 2009). Acute morphine administration can elevate locomotor activity (Mague et al, 2009), so we investigated if administration of sEVs from morphine-treated or control mice can impact locomotor activity in naïve recipient mice. We first confirmed successful injection of sEVs directly into the VTA. For this, sEVs were labeled with PKH67 green fluorescent membrane dye, and Fig. 6, A–C, shows successful infusion of sEVs. Our results show that injection of Mor-sEVs from the OIH pellet model does not impair the normal development of behavioral sensitization to morphine (Fig. 6D) in naïve sEV recipient mice.

3.6. sEVs do not induce a CPP

We have previously reported the successful delivery of dye-labeled sEVs to the spinal cord and dorsal root ganglion after intrathecal injections (Gupta et al, 2021; Jean-Toussaint et al, 2021). To determine whether sEVs from the morphine OIH model impacted locomotor behavior, the movement during the CPP and conditioning sessions was measured using consecutive beam breaks. The CPP paradigm is described in Fig. 7A. A repeated measures ANOVA (treatment day vs treatment group) indicated a main effect of treatment day, but no effect of treatment group or group \times day interaction, suggesting that sEVs did not significantly impact movement (Fig. 7B). Because overall movement was reduced on the second day of injections regardless of treatment group, this suggests that it was likely an effect of consecutive intrathecal injections (Supplemental Fig. 3). To determine whether

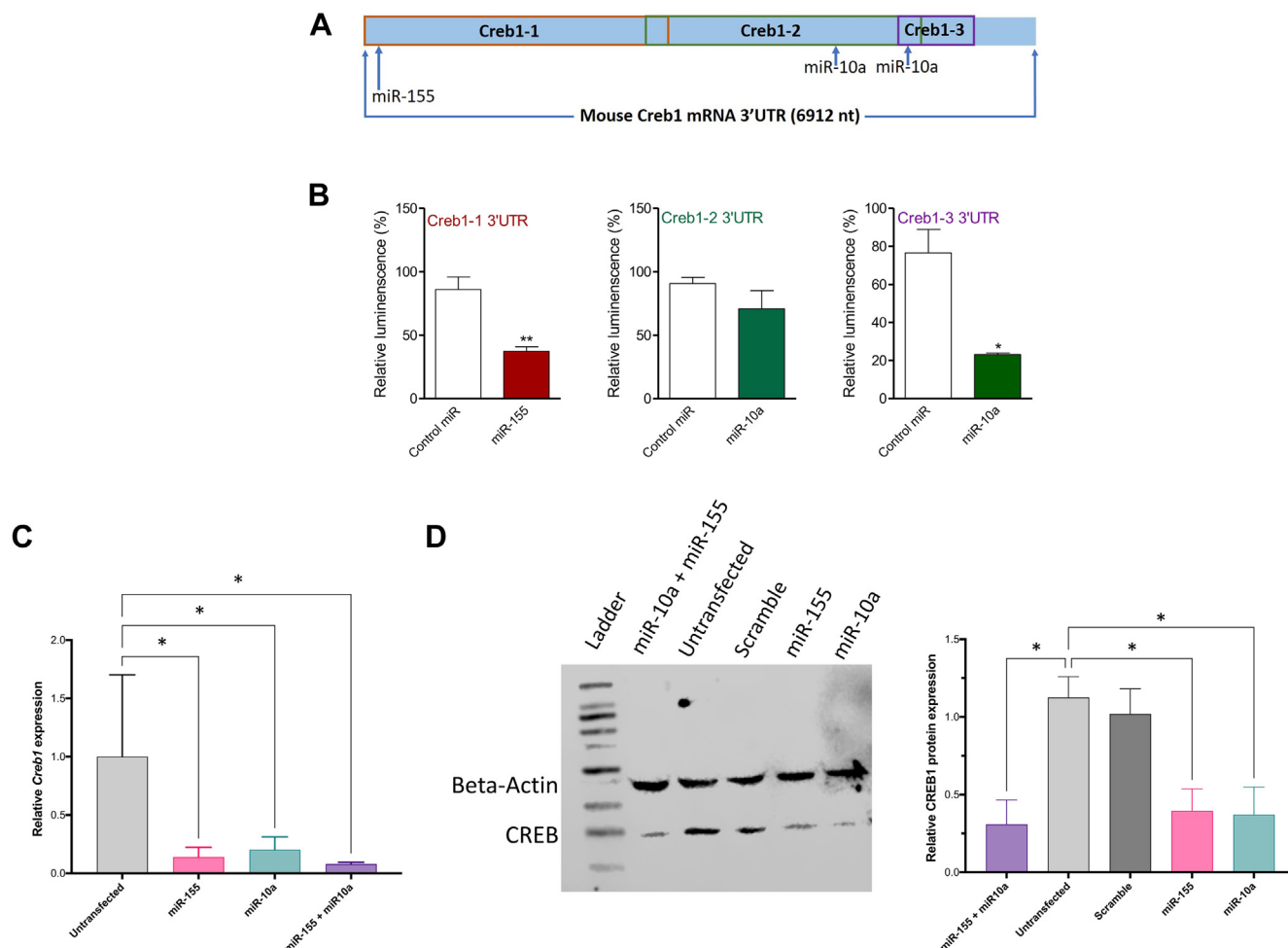


Fig. 4. Regulation of *Creb1* expression by miR-155 and miR-10a. (A) Schematic representation of miRNA target sites on *Creb1* mRNA 3'-UTR and the regions corresponding to 3'-UTR used in luciferase assay to validate mRNA-miRNA binding. (B) Confirmation of miR-155 and miR-10a binding to the 3'-UTR of *Creb1*. Reporter assay shows a significant reduction in relative luminescence in cells transfected with miR-10a or miR-155 in comparison to control miRNA, indicating that miR-155 and miR-10a can bind to *Creb1* 3'-UTR. * $P < .05$, ** $P < .005$, two-tailed unpaired t test. (C) TaqMan analysis of endogenous *Creb1* in RAW 264.7 cells 24 hours after transfection of miR-155, miR-10a, or both miRNAs. (D) Western blot analysis and quantification 24 hours after transfection of RAW 264.7 cells with miR-155, miR-10a, or both miRNAs significantly reduced CREB1 protein. Significance was determined using Student's t test, * $P < .05$.

sEV injection induced a preference for sEV-paired chambers, total time spent in each chamber was compared (Fig. 7C). As a biased design was used, CPP scores were calculated as time spent in the sEV-paired chamber after conditioning minus time spent prior to conditioning. No significant effect of sEV treatment was observed on CPP scores (one-way ANOVA) (Fig. 7D). Further, CPP scores did not significantly differ from zero for any of the treatment groups (1-sample t test), indicating that mice did not form a preference for sEV-paired chambers.

4. Discussion

We hypothesized that there would be distinct sEV miRNA signatures in prolonged morphine-treated mice, which may be involved in mediating the signaling related to substance use disorder and pain. Differential expression of miRNAs in males and females has been reported (Sharma and Eghbali, 2014; Guo et al, 2017; Zhong et al, 2023). In combining miRNAs detected in male and female mice, we found significant differential expression of 18 sEV miRNAs in the morphine-treated group compared with control mice. Pathway enrichment analysis for miRNAs differentially expressed in morphine-treated mice implicated

several pathways, including mTOR, MAPK, Wnt, and PI3K-Akt signaling, with MAPKs having the largest representation. MAPKs have a critical role in the signal transduction cascade associated with peripheral and central sensitization linked to the initiation and maintenance of chronic pain (Ji et al, 2009). Activation of the MAPK signaling pathway leads to the phosphorylation and activation of CREB and the transcription of pain-related genes. Increased CREB activation in neurons has been associated with heightened pain perception and the development of chronic pain. Phosphorylation of MAPKs and CREB is involved in the morphine-induced increase in spinal pain-related neuropeptides, calcitonin gene-related peptide, and substance P, levels in primary sensory afferents, contributing to the development of tolerance to opioid-induced analgesia (Ma et al, 2001). Also, chronic opioid use activates mTOR signaling, contributing to the development of hyperalgesia; repeated intrathecal administrations of morphine resulted in spinal dorsal horn mTOR activation through μ -opioid receptor-triggered PI3K/Akt signaling (Xu et al, 2014). Wnt proteins, through both canonical (β -catenin-dependent) and noncanonical pathways, contribute to pain sensitization, neuronal excitability, and neuroinflammation (Zhou et al, 2022). β -catenin can indirectly

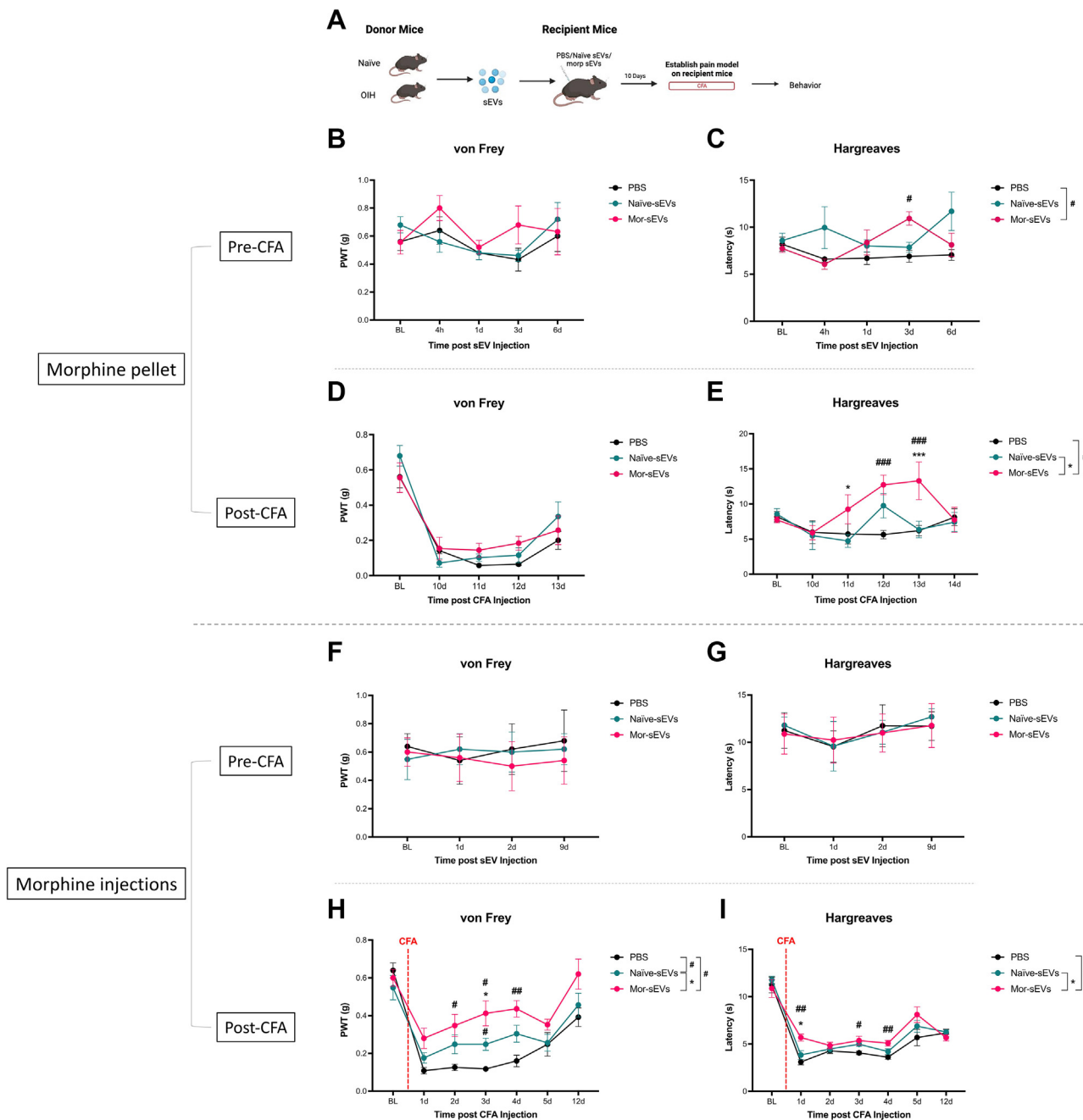


Fig. 5. Prophylactic intrathecal administration of sEVs isolated from the serum of chronic morphine-treated mice attenuates pain hypersensitivity. (A) Schematic representation of experimental design. After baseline behavioral testing, 1 μ g sEVs from male naive or morphine-treated donor mice, or PBS were injected intrathecally into 9-week-old male recipient mice. Mor-sEVs from morphine pellet model OIH mice did not alter basal (B) mechanical thresholds but increased basal (C) thermal thresholds 3 days after administration. Whereas, sEVs from morphine injection model mice did not alter either basal thresholds (F, G). The CFA model was established in recipient mice 10 days post sEV injection. Mechanical and thermal thresholds were assessed in recipient mice with sEVs from (D, E) morphine pellet and (H, I) repeated morphine injection OIH model mice. Statistical analysis was performed using repeated measures two-way ANOVA, data shown are mean \pm SEM (n = 5) * $^{\#}$ P < .05; ** $^{\#}$ P < .01; *** $^{\#}$ P < .001. BL, baseline; Mor, morphine; PWT, paw withdrawal threshold.

activate CREB by regulating signaling cascades such as PI3K/Akt and MAPK, both of which lead to CREB phosphorylation. Thus, Wnt signaling could enhance CREB-mediated transcription of genes involved in pain, such as *BDNF*, contributing to chronic pain states. Wnt signaling also plays a critical role in withdrawal symptoms from opioid receptor activation in mice (Wu et al, 2020). miRNAs altered in blood from multiple rodent models of pain, including neuropathic, inflammatory, and chemotherapy-

induced pain models, are predicted to target *Wnt* genes (Qureshi et al, 2016), suggesting downregulation of miRNAs that target Wnt may be a common mechanism in regulating pain.

Several of the miRNAs significantly altered in sEVs from morphine-treated mice that we identified were bioinformatically predicted to target *Creb1* 3'-UTR. We observed that *Creb1* is a validated target of miR-132 (Klein et al, 2007; Manners et al, 2015; Garcia-Concejo et al, 2016). We chose to focus on 2 miRNAs, miR-10

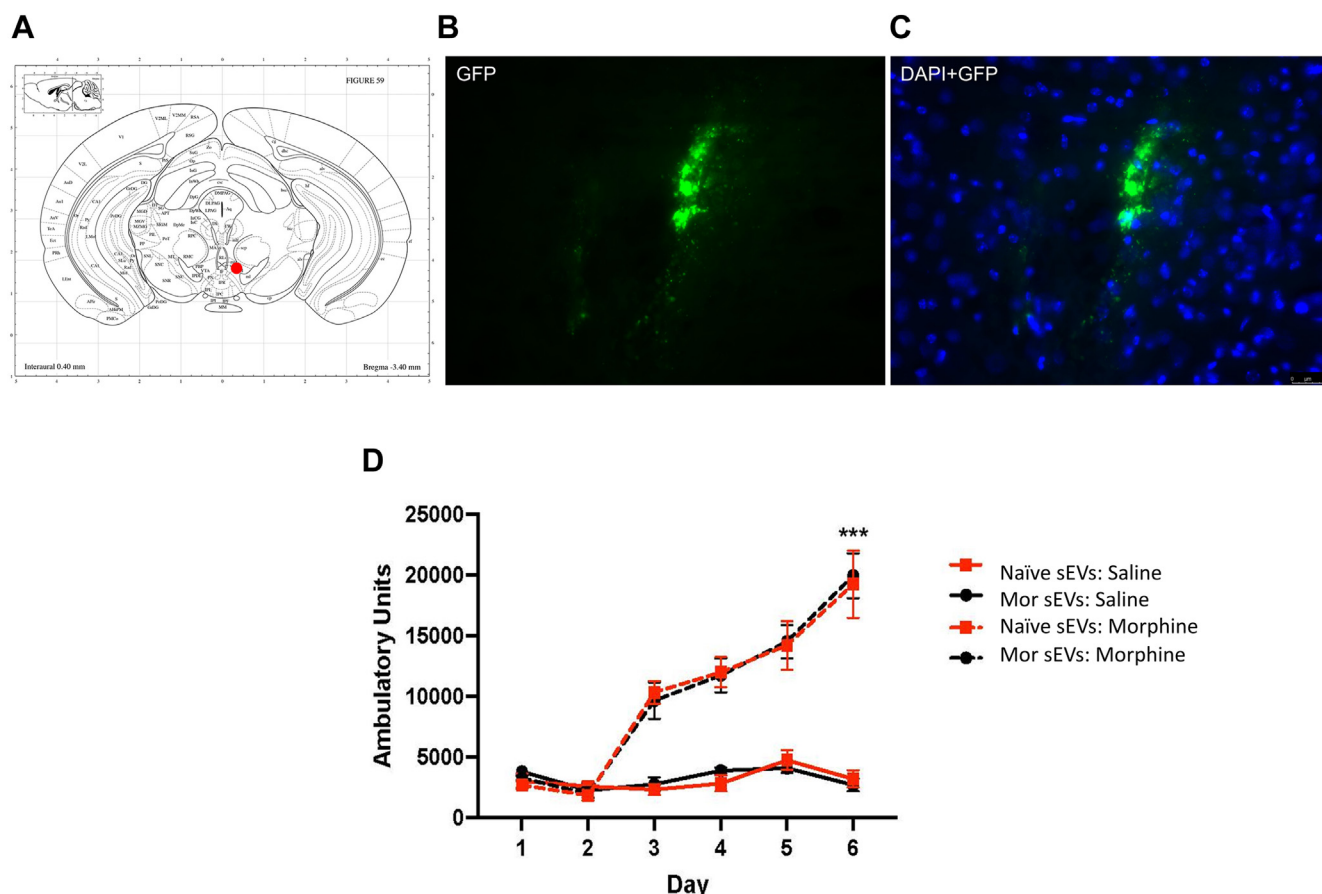


Fig. 6. Treatment with sEVs does not impair morphine-induced locomotor sensitization. Detection of PKH67-labeled sEVs in the mouse VTA (anteroposterior -3.4 , lateral -0.3 , and dorsoventral -4.4) 1 hour after infusion. (A) Schematic representation of the injection site. (B) PKH67 green label (C) PKH67 costained with DAPI (4',6-diamidino-2-phenylindole; blue). Images were taken at $40\times$ magnification. (D) sEVs from the morphine pellet-implanted OIH model injected directly into the VTA do not impair morphine-induced locomotor sensitization in C57BL/6J male mice. Saline was administered to both groups on days 1–3 and morphine (20 mg/kg) on days 3–6. The saline group received saline on all days, $n = 6$ /group. *** $P < .001$, main effect of group and morphine day 3 compared with day 6.

and miR-155, that were significantly upregulated in the morphine group compared with the control group. CREB is a well characterized transcription factor implicated in underlying mechanisms of both pain and drug addiction-related behaviors. A variety of addictive drugs have been shown to alter the expression and/or activation of CREB, and alterations in CREB activity are linked to behavioral manifestations of opioid reward, tolerance, and withdrawal (Maldonado et al, 1996; Walters and Blendy, 2001; Walters et al, 2005a,b). Morphine can alter the levels and function of CREB, and CREB signaling mediates a variety of morphine-induced behaviors. However, the mechanism of morphine-induced CREB regulation has been less well studied. We confirmed miRNA binding to the *Creb* 3'-UTR by luciferase reporter assay. Binding sites for miR-10a are present in fragments "2" and "3" which we generated for the ~ 7 kb long *Creb* 3'-UTR, but we observed more efficient binding of miRNAs to fragment "3" compared with fragment "2." Target locations are not evenly distributed throughout the whole UTR, and there is a strong preference for targets located in close vicinity to the stop codon and the polyadenylation sites (Bartel, 2009). This could contribute to the differences observed for miR-10a in our luciferase assays. Additionally, the role of RNA secondary structure in blocking miRNA access also cannot be ruled out. Downregulation of endogenously expressed mRNA and protein following miRNA transfection indicates that changes in CREB expression can be mediated by mRNA degradation or translational repression.

Studies have shown significant differences between the populations of miRNAs in cells and their secreted sEVs (Honegger et al, 2015; Huang et al, 2018; Statello et al, 2018). Thus, miRNA availability for secretion in sEVs is controlled, at least in part, by the cellular levels of their targeted transcripts (Squadrito et al, 2014; Ramanathan et al, 2019b). Our previous studies using mouse cortical neurons and astrocytes showed that only 20.7% of astrocyte-derived miRNAs were loaded into sEVs, while 41.0% of neuron-derived miRNAs were loaded into sEVs (Luo et al, 2021), indicating differences and specificity in the cellular sorting mechanisms and that cargo loading into sEVs is a highly regulated process. Our results here demonstrate that chronic morphine alters sEV composition. Previous miRNA profiling of sEVs from morphine-treated astrocytes showed enrichment of miRNAs with an adenine and uracil- or guanine and uracil-rich motif (Hu et al, 2018). Because it is challenging to determine the source of sEVs in circulation, future studies will determine how morphine treatment can impact this packaging along with the role of specific motifs and RNA-binding proteins in determining selective sorting of miRNAs into sEVs.

To investigate the functional impact of transferring sEVs from the OIH model to naïve mice, we intrathecally injected $1\ \mu\text{g}$ of Mor-sEVs into naïve recipient mice. Mor-sEVs from the morphine pellet-implanted but not the morphine injection model of OIH donor mice resulted in an elevated thermal pain threshold in naïve recipient mice on day 3. sEVs from control mice did not induce any

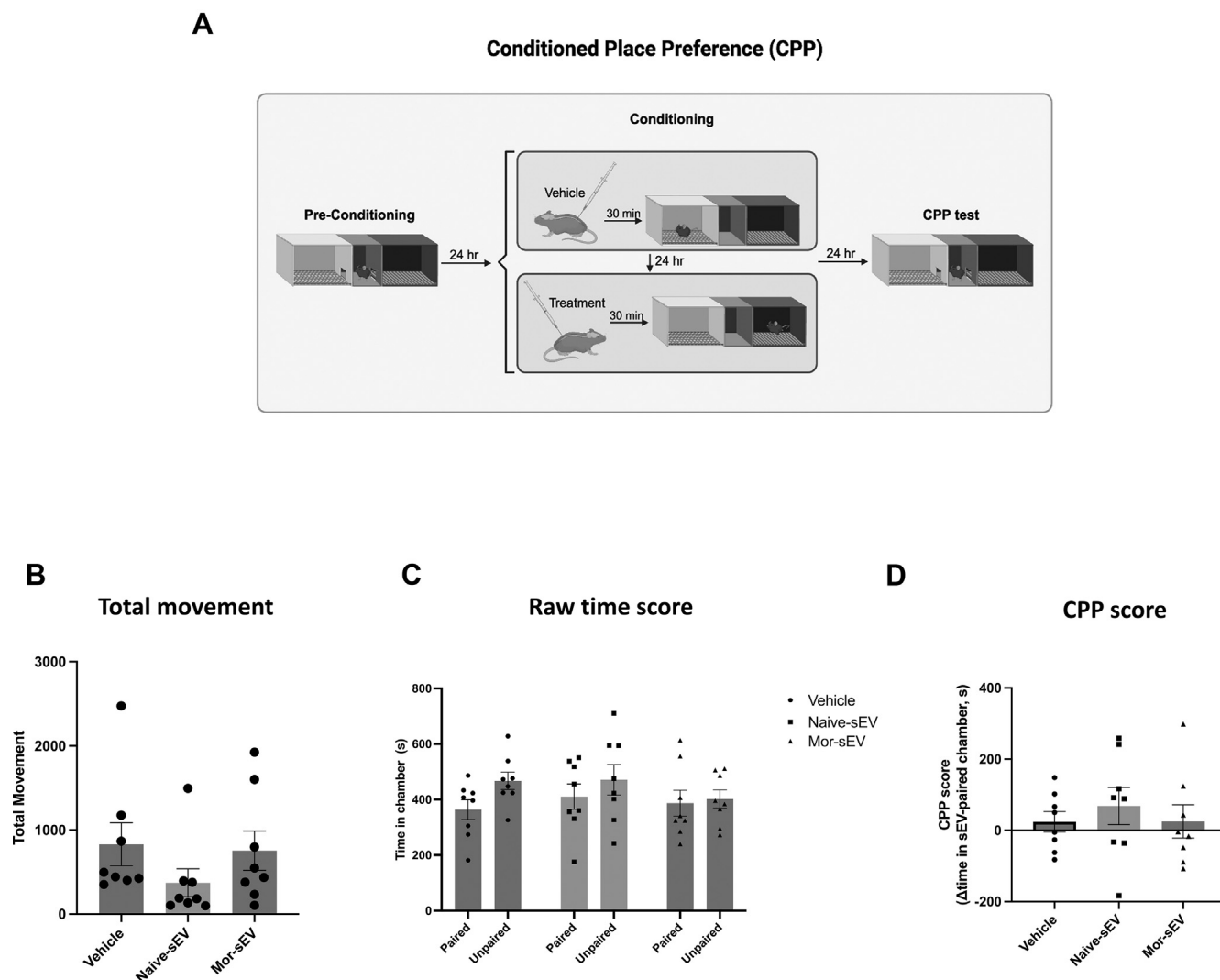


Fig. 7. sEV treatment does not induce a CPP. (A) Schematic representation of the CPP paradigm. (B) Total movement did not significantly differ between groups, suggesting sEVs from the morphine injection model of OIH do not impair movement. (C) Total time in chambers and (D) CPP scores did not differ between vehicle or sEV-treated mice. No groups exhibited a CPP score significantly different from zero, suggesting that sEV treatment did not elicit a CPP. Statistical analysis was performed using one-way ANOVA and one-sample *t* test, bars represent mean \pm SEM ($n = 8$).

alterations in basal mechanical or thermal thresholds at 1 μ g as we reported previously (Lin et al, 2025). We next assessed if prophylactic Mor-sEVs can induce faster resolution of inflammatory pain as observed previously with 1 μ g RAW 264.7 macrophage cell line-derived sEVs (Jean-Toussaint et al, 2021) and 10 μ g of mouse serum-derived sEVs (naïve and neuropathic pain model mice) (Lin et al, 2025). Interestingly, 1 μ g of serum-derived Mor-sEVs from both morphine pellet and injection models of OIH showed an earlier resolution of CFA-induced thermal hypersensitivity in naïve recipient mice. Mor-sEVs from the morphine injection OIH model also resulted in earlier resolution of mechanical hypersensitivity. Collectively, our studies show that 1 μ g sEVs from the OIH model was more efficacious in inducing behavioral changes in recipient mice compared with sEVs from the serum of naïve control mice or the spared nerve injury model of neuropathic pain (Lin et al, 2025). How different morphine treatment paradigms impact the composition of miRNAs and other sEV cargo in circulation and how the uptake of these sEVs by recipient cells contributes to behavioral responses underlying inflammatory pain remain to be elucidated. Pathway analysis of miRNAs altered in blood from rodent models of pain (Qureshi et al, 2016) suggests that there could be shared

mechanisms such as regulation of Wnt signaling. We found that administering sEVs from morphine-treated mice does not impair the normal development of behavioral sensitization in recipient mice, and sEVs do not impact subsequent response to morphine in recipient mice. We used sEVs from the morphine pellet-implanted OIH model for the locomotor sensitization test, and because we did not see an effect, we tested sEVs from the repeated morphine injection model for the CPP test. These sEVs did not induce a CPP in recipient mice. We also did not observe any aversive learning associated with sEV administration, suggesting that sEVs did not induce conditioned place aversion either.

We used male and female mice for miRNA profiling, but all the recipient mice used were male. Morphine is more potent in males compared with females, and these sex differences in opioid analgesia have been attributed to higher levels of mu-opioid receptor expression and binding in males (Averitt et al, 2019). Future studies matching the sexes of sEV donor and recipient mice will help elucidate if there are sex-specific differences in sEV function. Another limitation of our studies is that we used only 1 μ g sEVs, and this potentially resulted in modest behavior effects in recipient mice. Using higher concentrations of sEVs may produce more robust behavior

outcomes in sEV recipient mice. A major challenge for successful translation remains the difficulty in precisely targeting the cell type or organ of interest while limiting off-target biodistribution. We have previously reported the presence of endogenous opioids, specifically leu-enkephalin, in serum-derived sEVs (Lin et al, 2025). It will be interesting to investigate how morphine treatment impacts the packaging and thus the sEV composition of endogenous opioids in OIH models. In sum, our data indicate that administration of 1 μ g sEVs from OIH models can induce desired behavioral outcomes in vivo, ie, a protective role for sEVs from morphine-treated mice in attenuating pain hypersensitivity without augmenting behaviors associated with opioid use disorders. As CREB is not a “druggable” target, the potential to modulate its expression in vivo with sEVs could prove to be an innovative approach to regulating gene expression.

Abbreviations

CFA, complete Freund's adjuvant; CPP, conditioned place preference; CT, cycle threshold; DPBS, Dulbecco's PBS; EV, extracellular vesicle; GO, Gene Ontology; MFI, mean fluorescence intensity; miRNA, microRNA; Mor-sEVs, morphine-derived small extracellular vesicles; OIH, opioid-induced hyperalgesia; %Pos, positive percentage; qPCR, quantitative polymerase chain reaction; sEV, small extracellular vesicle; TBST, Tris-buffered saline with Tween detergent; UTR, untranslated region; VTA, ventral tegmental area.

Acknowledgments

We thank Julia K. Brynildsen for stereotaxic injections of sEV into the VTA and locomotor behavior assay.

Financial support

This study was partially supported by the National Institutes of Health National Institute of Neurological Disorders and Stroke [Grants R01 NS102836, R01NS129191, and 1R1NS130481] (to S.K.A.) and the National Institutes of Health National Institute on Alcohol Abuse and Alcoholism [Grant R21 AA030823] (to J.M.B.). D.R., X.L., and R.P. received Dean's Fellowship for Excellence in Collaborative or Themed Research from Drexel University College of Medicine.

Conflict of interest

No author has an actual or perceived conflict of interest with the contents of this article.

Data availability

The authors declare that all the data supporting the findings of this study are contained within the paper.

Authorship contributions

Participated in research design: Reddy, Lin, Ramanathan, Luo, Barker, Sacan, Blendy, and Ajit.

Conducted experiments: Reddy, Lin, Ramanathan, Luo, Pande, Tian, and Side.

Performed data analysis: Reddy, Lin, Ramanathan, Luo, Pande, Barker, Sacan, Blendy, Ajit.

Wrote or contributed to the writing of the manuscript: Reddy, Ramanathan, Luo, Barker, Sacan, Blendy, Ajit.

Supplemental material

This article has supplemental material available at jpet.aspetjournals.org.

References

- Angst MS and Clark JD (2006) Opioid-induced hyperalgesia: a qualitative systematic review. *Anesthesiology* **104**:570–587.
- Arout CA, Edens E, Petrakis IL, and Sofuoglu M (2015) Targeting opioid-induced hyperalgesia in clinical treatment: neurobiological considerations. *CNS Drugs* **29**:465–486.
- Averitt DL, Eidson LN, Doyle HH, and Murphy AZ (2019) Neuronal and glial factors contributing to sex differences in opioid modulation of pain. *Neuropsychopharmacology* **44**:155–165.
- Bannon AW and Malmberg AB (2007) Models of nociception: hot-plate, tail-flick, and formalin tests in rodents. *Curr Protoc Neurosci* **Chapter 8**:Unit 8.9.
- Bartel DP (2009) MicroRNAs: target recognition and regulatory functions. *Cell* **136**:215–233.
- Caobi A, Bonilla J, Gomez M, Andre M, Yndart A, Fernandez-Lima FA, Nair MP, and Raymond AD (2023) HIV-1 and opiates modulate miRNA profiles in extracellular vesicles. *Front Immunol* **14**:1259998.
- Chen Y, Yang C, and Wang ZJ (2010) Ca²⁺/calmodulin-dependent protein kinase II α is required for the initiation and maintenance of opioid-induced hyperalgesia. *J Neurosci* **30**:38–46.
- Chu LF, Angst MS, and Clark D (2008) Opioid-induced hyperalgesia in humans: molecular mechanisms and clinical considerations. *Clin J Pain* **24**:479–496.
- Colvin LA, Bull F, and Hales TG (2019) Perioperative opioid analgesia-when is enough too much? A review of opioid-induced tolerance and hyperalgesia. *Lancet* **393**:1558–1568.
- Couch Y, Buzás EI, Di Vizio D, Gho YS, Harrison P, Hill AF, Lötvall J, Raposo G, Stahl PD, Théry C, et al (2021) A brief history of nearly EV-erything—the rise and rise of extracellular vesicles. *J Extracell Vesicles* **10**:e12144.
- D'Agnelli S, Gerra MC, Bignami E, and Arendt-Nielsen L (2020) Exosomes as a new pain biomarker opportunity. *Mol Pain* **16**:1744806920957800.
- Deuis JR, Dvorakova LS, and Vetter I (2017) Methods used to evaluate pain behaviors in rodents. *Front Mol Neurosci* **10**:284–284.
- Garcia-Concejo A, Jimenez-Gonzalez A, and Rodriguez RE (2016) μ opioid receptor expression after morphine administration is regulated by miR-212/132 Cluster. *PLoS One* **11**:e0157806.
- Ge SX, Jung D, and Yao R (2020) ShinyGO: a graphical gene-set enrichment tool for animals and plants. *Bioinformatics* **36**:2628–2629.
- Gereau RW IV, Sluka KA, Maixner W, Savage SR, Price TJ, Murinson BB, Sullivan MD, and Fillingim RB (2014) A pain research agenda for the 21st century. *J Pain* **15**:1203–1214.
- Guo L, Zhang Q, Ma X, Wang J, and Liang T (2017) miRNA and mRNA expression analysis reveals potential sex-biased miRNA expression. *Sci Rep* **7**:39812.
- Gupta R, Luo X, Lin Z, Tian Y, and Ajit SK (2021) Uptake of fluorescent labeled small extracellular vesicles in vitro and in spinal cord. *J Vis Exp*. <https://doi.org/10.3791/62537>.
- Hartmann A, Muth C, Dabrowski O, Krasemann S, and Glatzel M (2017) Exosomes and the prion protein: more than one truth. *Front Neurosci* **11**, 194–194.
- Honegger A, Schilling D, Bastian S, Sponagel J, Kuryshv V, Sultmann H, Scheffner M, Hoppe-Seyler K, and Hoppe-Seyler F (2015) Dependence of intracellular and exosomal microRNAs on viral E6/E7 oncogene expression in HPV-positive tumor cells. *PLoS Pathog* **11**:e1004712.
- Hornung S, Dutta S, and Bitan G (2020) CNS-derived blood exosomes as a promising source of biomarkers: opportunities and challenges. *Front Mol Neurosci* **13**:38.
- Hu G, Liao K, Niu F, Yang L, Dallon BW, Callen S, Tian C, Shu J, Cui J, Sun Z, et al (2018) Astrocyte EV-induced lincRNA-Cox2 regulates microglial phagocytosis: implications for morphine-mediated neurodegeneration. *Mol Ther Nucleic Acids* **13**:450–463.
- Huang HY, Lin YCD, Cui S, Huang Y, Tang Y, Xu J, Bao J, Li Y, Wen J, Zuo H, et al (2022) miRTarBase update 2022: an informative resource for experimentally validated miRNA-target interactions. *Nucleic Acids Res* **50**:D222–D230.
- Huang Q, Yang J, Zheng J, Hsueh C, Guo Y, and Zhou L (2018) Characterization of selective exosomal microRNA expression profile derived from laryngeal squamous cell carcinoma detected by next generation sequencing. *Oncol Rep* **40**:2584–2594.
- Jean-Toussaint R, Lin Z, Tian Y, Gupta R, Pande R, Luo X, Hu H, Sacan A, and Ajit SK (2021) Therapeutic and prophylactic effects of macrophage-derived small extracellular vesicles in the attenuation of inflammatory pain. *Brain Behav Immun* **94**:210–224.
- Ji RR, Gereau RW, Malcangio M, and Strichartz GR (2009) MAP kinase and pain. *Brain Res Rev* **60**:135–148.
- Kim SH, Lechman ER, Bianco N, Menon R, Keravala A, Nash J, Mi Z, Watkins SC, Gambotto A, and Robbins PD (2005) Exosomes derived from IL-10-treated dendritic cells can suppress inflammation and collagen-induced arthritis. *J Immunol* **174**:6440–6448.

- Klein ME, Lioy DT, Ma L, Impey S, Mandel G, and Goodman RH (2007) Homeostatic regulation of MeCP2 expression by a CREB-induced microRNA. *Nat Neurosci* **10**: 1513–1514.
- Lee M, Silverman SM, Hansen H, Patel VB, and Manchikanti L (2011) A comprehensive review of opioid-induced hyperalgesia. *Pain Physician* **14**: 145–161.
- Li X, Angst MS, and Clark JD (2001) A murine model of opioid-induced hyperalgesia. *Brain Res Mol Brain Res* **86**:56–62.
- Liang DY, Li WW, Nwaneshiudu C, Irvine KA, and Clark JD (2019) Pharmacological characters of oliceridine, a μ -opioid receptor g-protein-biased ligand in mice. *Anesth Analg* **129**:1414–1421.
- Liang D, Shi X, Qiao Y, Angst MS, Yeomans DC, and Clark JD (2008) Chronic morphine administration enhances nociceptive sensitivity and local cytokine production after incision. *Mol Pain* **4**:7.
- Liao K, Niu F, Hu G, and Buch S (2022) Morphine-mediated release of astrocyte-derived extracellular vesicle miR-23a induces loss of pericyte coverage at the blood-brain barrier: implications for neuroinflammation. *Front Cell Dev Biol* **10**: 984375.
- Lin Z, Luo X, Wickman JR, Reddy D, DaCunza JT, Pande R, Tian Y, Kasimoglu EE, Triana V, Lee J, et al (2025) Inflammatory pain resolution by mouse serum-derived small extracellular vesicles. *Brain Behav Immun* **123**:422–441.
- Luo X, Jean-Toussaint R, Sacan A, and Ajit SK (2021) Differential RNA packaging into small extracellular vesicles by neurons and astrocytes. *Cell Commun Signal* **19**: 75.
- Ma W, Zheng WH, Powell K, Jhamandas K, and Quirion R (2001) Chronic morphine exposure increases the phosphorylation of MAP kinases and the transcription factor CREB in dorsal root ganglion neurons: an in vitro and in vivo study. *Eur J Neurosci* **14**:1091–1104.
- Mague SD, Isiegas C, Huang P, Liu-Chen LY, Lerman C, and Blendy JA (2009) Mouse model of OPRM1 (A118G) polymorphism has sex-specific effects on drug-mediated behavior. *Proc Natl Acad Sci U S A* **106**:10847–10852.
- Maldonado R, Blendy JA, Tzavara E, Gass P, Roques BP, Hanoune J, and Schütz G (1996) Reduction of morphine abstinence in mice with a mutation in the gene encoding CREB. *Science* **273**:657–659.
- Manners MT, Tian Y, Zhou Z, and Ajit SK (2015) MicroRNAs downregulated in neuropathic pain regulate MeCP2 and BDNF related to pain sensitivity. *FEBS Open Bio* **5**:733–740.
- McDonald MK, Tian Y, Qureshi RA, Gormley M, Ertel A, Gao R, Aradillas Lopez E, Alexander GM, Sacan A, Fortina P, et al (2014) Functional significance of macrophage-derived exosomes in inflammation and pain. *Pain* **155**:1527–1539.
- McGeary SE, Lin KS, Shi CY, Pham TM, Bisaria N, Kelley GM, and Bartel DP (2019) The biochemical basis of microRNA targeting efficacy. *Science* **366**: eaav1741.
- Odegaard KE, Chand S, Wheeler S, Tiwari S, Flores A, Hernandez J, Savine M, Gowen A, Pendyala G, and Yelamanchili SV (2020) Role of extracellular vesicles in substance abuse and HIV-related neurological pathologies. *Int J Mol Sci* **21**: 6765.
- Ossipov MH, Lai J, King T, Vanderah TW, Malan TP Jr, Hruby VJ, and Porreca F (2004) Antinociceptive and nociceptive actions of opioids. *J Neurobiol* **61**:126–148.
- Paxinos G and Franklin KBJ (2007) *The Mouse Brain in Stereotaxic Coordinates*. Elsevier Science, Amsterdam, Netherlands.
- Qureshi RA, Tian Y, McDonald MK, Capasso KE, Douglas SR, Gao R, Orlova IA, Barrett JE, Ajit SK, and Sacan A (2016) Circulating microRNA signatures in rodent models of pain. *Mol Neurobiol* **53**:3416–3427.
- Ramanathan S, Douglas SR, Alexander GM, Shenoda BB, Barrett JE, Aradillas E, Sacan A, and Ajit SK (2019a) Exosome microRNA signatures in patients with complex regional pain syndrome undergoing plasma exchange. *J Transl Med* **17**: 81.
- Ramanathan S, Shenoda BB, Lin Z, Alexander GM, Huppert A, Sacan A, and Ajit SK (2019b) Inflammation potentiates miR-939 expression and packaging into small extracellular vesicles. *J Extracell Vesicles* **8**:1650595.
- Robinson TE and Berridge KC (1993) The neural basis of drug craving: an incentive-sensitization theory of addiction. *Brain Res Brain Res Rev* **18**:247–291.
- Roeckel LA, Le Coz GM, Gavériaux-Ruff C, and Simonin F (2016) Opioid-induced hyperalgesia: cellular and molecular mechanisms. *Neuroscience* **338**:160–182.
- Schmittgen TD and Livak KJ (2008) Analyzing real-time PCR data by the comparative C(T) method. *Nat Protoc* **3**:1101–1108.
- Sharma S and Eghbali M (2014) Influence of sex differences on microRNA gene regulation in disease. *Biol Sex Differ* **5**:3.
- Squadrino ML, Baer C, Burdet F, Maderna C, Gilfillan GD, Lyle R, Ibberson M, and De Palma M (2014) Endogenous RNAs modulate microRNA sorting to exosomes and transfer to acceptor cells. *Cell Rep* **8**:1432–1446.
- Statello L, Maugeri M, Garre E, Nawaz M, Wahlgren J, Papadimitriou A, Lundqvist C, Lindfors L, Collén A, Sunnerhagen P, et al (2018) Identification of RNA-binding proteins in exosomes capable of interacting with different types of RNA: RBP-facilitated transport of RNAs into exosomes. *PLoS One* **13**:e0195969.
- Thery C, Ostrowski M, and Segura E (2009) Membrane vesicles as conveyors of immune responses. *Nat Rev Immunol* **9**:581–593.
- van Niel G, D'Angelo G, and Raposo G (2018) Shedding light on the cell biology of extracellular vesicles. *Nat Rev Mol Cell Biol* **19**:213–228.
- Walters CL and Blendy JA (2001) Different requirements for cAMP response element binding protein in positive and negative reinforcing properties of drugs of abuse. *J Neurosci* **21**:9438–9444.
- Walters CL, Cleck JN, Kuo YC, and Blendy JA (2005a) Mu-opioid receptor and CREB activation are required for nicotine reward. *Neuron* **46**:933–943.
- Walters CL, Godfrey M, Li X, and Blendy JA (2005b) Alterations in morphine-induced reward, locomotor activity, and thermoregulation in CREB-deficient mice. *Brain Res* **1032**:193–199.
- Walters CL, Wang BC, Godfrey M, Sun D, Funk CD, and Blendy JA (2003) Augmented responses to morphine and cocaine in mice with a 12-lipoxygenase gene disruption. *Psychopharmacology (Berl)* **170**:124–131.
- Wilczynska A and Bushell M (2015) The complexity of miRNA-mediated repression. *Cell Death Differ* **22**:22–33.
- Wu M, Li Z, Liang L, Ma P, Cui D, Chen P, Wu G, and Song XJ (2020) Wnt signaling contributes to withdrawal symptoms from opioid receptor activation induced by morphine exposure or chronic inflammation. *Pain* **161**:532–544.
- Xu JT, Zhao JY, Zhao X, Ligons D, Tiwari V, Atianjoh FE, Lee CY, Liang L, Zang W, Njoku D, et al (2014) Opioid receptor-triggered spinal mTORC1 activation contributes to morphine tolerance and hyperalgesia. *J Clin Invest* **124**: 592–603.
- Zappulli V, Friis KP, Fitzpatrick Z, Maguire CA, and Breakefield XO (2016) Extracellular vesicles and intercellular communication within the nervous system. *J Clin Invest* **126**:1198–1207.
- Zhong B, Cui C, and Cui Q (2023) Identification and analysis of sex-biased microRNAs in human diseases. *Genes (Basel)* **14**:1688.
- Zhou YQ, Tian XB, Tian YK, Mei W, Liu DQ, and Ye DW (2022) Wnt signaling: a prospective therapeutic target for chronic pain. *Pharmacol Ther* **231**: 107984.